Strength Behavior of Temperature-Dependent MICP-Treated Soil

Yuze Wang*, Yong Wang, Charalampos Konstantinou

To cite this article: Wang Y, Wang Y, Konstantinou C. Strength Behavior of Temperature-Dependent MICP-Treated Soil. *ASCE Journal of Geotechnical and Geoenvironmental Engineering*, **2023-9-28**. DOI: 10.1061/JGGEFK.GTENG-11526.

To link to this article:：https://ascelibrary.org/doi/10.1061/JGGEFK.GTENG-11526

Strength behavior of temperature-dependent Microbially Induced Carbonate Precipitation (MICP)-treated soil

Yuze Wang[a,b]*, Yong Wang[b], Charalampos Konstantinou[c]

a. Shenzhen Key Laboratory of Natural Gas Hydrates, Southern University of Science and Technology, Shenzhen, 518055, China;

b. Department of Ocean Science and Engineering, Southern University of Science and Technology, Shenzhen, 518055, China;

c. Department of Civil and Environmental Engineering, University of Cyprus, Nicosia, Cyprus

Corresponding author: Yuze Wang; email address: wangyz@sustech.edu.cn

Abstract

Microbially Induced Carbonate Precipitation (MICP) is a novel soil strengthening technique that involves a bio-geo-chemical process. Temperature plays a crucial role in influencing the biological and chemical processes involved in the formation of carbonate precipitates, which in turn affect the mechanical properties of the treated soil. The aim of this study was to investigate the impact of temperature on the cementing structure of MICP-treated soils and its subsequent effects on their strength parameters. The results revealed that temperature considerably affected the content, size, and distribution of $CaCO_3$ crystals produced, resulting in variations in the friction angle, cohesion, stiffness, peak strength, residual strength, and dilation of the MICP-treated soil samples. Lower strength enhancement was observed when fewer and smaller carbonate crystals were produced at

4°C and 50°C. In contrast, higher numbers of larger crystal clusters were produced at 20°C and 35°C, which effectively bonded the soil particles. Increasing the number of bacterial injections at 50°C promoted the formation of larger crystals and enhanced strength effectively. This study highlights the temperature effects on calcium carbonate growth in biocemented soils, which is a critical step in determining the field-scale application of this innovative soil stabilization technique.

Keywords: environmental temperature; urease activity; MICP performance; consolidated drained triaxial tests

1 Introduction

Microbially Induced Carbonate Precipitation (MICP) is a biochemical process that involves microorganisms inducing an enzyme-catalyzed reaction to increase the supersaturation ratio of carbonate minerals, such as calcium carbonate, and causing their precipitation in an aqueous environment within soil pores or geo-structure cracks (Mitchell and Santamarina 2005; DeJong et al. 2006). The solid surfaces of soil particles or geo-structures provide the nucleation sites for $CaCO_3$ crystal formation. Among the various MICP processes for soil stabilization, ureolysis-driven MICP is the most extensively studied, owing to its high chemical conversion efficiency and ease of control. In this process, ureolytic bacterial cells are introduced into the soil matrix through either bio-augmentation or bio-stimulation (Gomez et al. 2017; Graddy et al. 2021), followed by multiple injections of cementation solution containing $CaCl_2$, urea and nutrient broth. Ureolysis bacteria express urease enzyme, which catalyzes the hydrolysis of urea (*Equation 1*). The addition of calcium (Ca^{2+}) to this system induces the precipitation of calcium carbonate ($CaCO_3$) as the CO_3^{2-} ions produced by the hydrolysis of urea react with the supplied Ca^{2+} (*Equation 2*), whilst the addition of nutrient broth to this system maintains the bacterial activity throughout the precipitation period:

$$CO(NH_2)_2 + 2H_2O \xrightarrow{Urease} 2NH_4^{+} + CO_3^{2-} \quad (1)$$

$$Ca^{2+} + CO_3^{2-} \rightarrow CaCO_3(s) \quad (2)$$

The precipitated $CaCO_3$ crystals bind the soil particles, increasing soil strength and stiffness, whilst maintaining a relatively high soil permeability, or filling the cracks in geo-structures and reducing their permeability (Wang et al. 2023). Therefore, MICP has many applications such as soil stabilisation (DeJong et al., 2006, 2010; van Paassen et al. 2010; Naveed et al. 2019), production of cemented sandstones (Konstantinou et al. 2021a), improvement of liquefaction resistance (Montoya et al. 2013; Xiao et al. 2018; Darby et al. 2019), control of soil erosion (Jiang et al. 2017; Chek et al. 2021), maintenance of wellbore integrity, fracture sealing (Cuthbert et al. 2013; Phillips et al. 2018), and the modification and protection of materials (Tobler et al. 2018). Moreover, MICP has been suggested for producing energy piles (Venuleo et al. 2016; Martinez et al. 2019), preventing the corrosion of marine materials (Guo et al. 2019), separating oil and water (Tang et al. (2021), forming deep foundations (Lin et al. 2016, 2021; Zamani et al. 2021), stabilizing gas hydrate-bearing sediments (Hata et al. 2020), and achieving ocean negative carbon emission (Zhang et al. 2022).

As the use of Microbially Induced Carbonate Precipitation (MICP) expands and its applications extend to various environmental conditions, the impact of factors such as pH, salinity, oxygen level, and temperature on its effectiveness must be considered. Of these, temperature is a critical factor.

Despite the fact that various studies have shown that soil engineering properties, such as strength, stiffness, deformation, and creep behavior, are minimally affected by temperature within the range of room temperature to 90°C (Burghignoli et al. 1999; Liu et al. 2018), the impact of environmental temperature on the effectiveness of MICP for soil stabilization is significant. This is mainly because temperature affects the processes involved in MICP and the properties of carbonate crystals, which indirectly impact the engineering behavior of MICP-treated soils. For instance, Cheng et al. (2017) reported that 25°C was more efficient than 4°C and 50°C in generating the largest $CaCO_3$ crystals and achieving the highest unconfined compressive strength (UCS) of MICP-treated soils. In addition, earlier studies have shown that crystal number and characteristics were considerably influenced by bacterial quantity and crystal growth dynamics, which were highly dependent on temperature in the range of 4-50°C (Wang et al. 2022a).

Based on these findings, it is crucial to further investigate the impact of treatment temperature on the cementing structure in MICP-treated soils, and how this influences their strength parameters. Given that MICP is employed in a wide range of applications, from stabilization of gas hydrate-bearing sediments where temperatures can range from 3.5 to 14.5°C at the seafloor (Fujii et al., 2015; Li et al., 2018; Ye et al., 2020), to energy piles where temperatures can reach 30°C at shallow depths and 80°C at higher depths, and wellbore integrity and fracture sealing where temperatures can be 35-55°C (Toribio et al. 2004) or even reaching or exceed 100°C based on typical geothermal gradients (Tian et al. 2015; Jing et al. 2022) , this study focuses on a series of MICP treatment tests conducted within the temperature range of 4-50°C. To investigate the strength parameters of MICP-treated soils, triaxial tests are essential. Previous studies have examined the strength parameters of soil after treatment at room temperature, such as Montoya and DeJong (2015), Cui et al. (2017), Gao et al. (2019), and Nafisi et al. (2020). However, in this study, MICP is carried out at various temperatures, and triaxial tests are performed to obtain the strength parameters of MICP-treated samples, which was not conducted previously. Additionally, SEM imaging and X-ray diffraction (XRD) analysis are used to analyze the effects of temperature and extra bacterial injections on calcium carbonate crystals and their impact on soil parameters. This study discusses the implications of these findings for resulting engineering properties and treatment protocols for subsurface applications of MICP.

2 Materials and methods

2.1 Sand properties and specimen preparation

In this study, a fine silica sand conforming to the CHINA ISO standard was employed. The sand has an average grain size of 0.125 mm and a coefficient of uniformity, Cu of 5.6, as depicted in Fig.1. Based on the Unified Soil Classification System (ASTM, 2017), the sand is classified as poorly graded. To prepare the samples, split acrylic cylindrical molds with an inner diameter of 38 mm and a height of 80 mm were used (Fig. 2a). The weight of the dry sand was calculated to achieve a targeted relative density (RD) of 50%. The sand was poured into the columns using a dry pluviation method. The sand columns were then flushed multiple times with deionized water to remove any air present until the flow rate stabilized and the specimen became completely saturated. The outlet tube was closed with a drain valve to maintain the sand column's saturation until the biotreatment process was initiated.

2.2 Biological suspension and cementation solution

The urease-active strain *S. pasteurii* (CGMCC1.3687) was chosen in this study, as it has demonstrated superior urease activity compared to many other alternative ureolytic bacteria. The strain was cultivated in a NH_4-YE liquid media (ATCC 1366) comprising 20 g/L yeast extract, 10 g/L ammonium sulfate, and 0.13 M tris buffer at 30°C for approximately 24 hours in a shaking incubator at 200 rpm/min until it reached an optical density at 600 nm (OD_{600}) of 1.0. The bacterial activity of the bacterial suspension tested at OD_{600} of 1.0 was approximately 40 mM/h. The cementation solution used consisted of 0.75 M urea, 0.5 M calcium chloride, and 3 g/L nutrient broth. A urea to calcium chloride ratio greater than one was chosen as previous studies have demonstrated its greater effectiveness (Montoya et al. 2013, 2015; Martinez et al. 2013). All chemical reagents used in this study were of analytical grade.

2.3 MICP treatment

A gravity filtration method was used for the MICP treatment process, where injection was performed from the top to the bottom using gravity (see Figure 2a and b). The staged injection method was employed for the MICP treatment, and the MICP treatment parameters are listed in Table 1. To improve bacterial attachment to soil particles, a 24-hour retention period was utilized for Test No. 1-4. Additionally, a 24-hour bacterial settling time was chosen to enhance bacterial settlement and distribution homogeneity (Wang 2022a, b; Konstantinou et al. 2021). As bacterial urease activity decreases rapidly at 50°C (Wang et al. 2022a), the number of bacterial suspension (BS) injections at 50°C was increased to 3 and 6, respectively, in groups 5 and 6. Moreover, the time between BS and cementation solution (CS) injections was reduced to 2 hours instead of 24 hours in these two tests. In all tests, 1.0 pore volume (PV) of BS or CS were injected each time, and the total number of CS injections was 6. During the retention times of the experiment, the samples were kept at the specified temperature. To achieve four temperatures (4°C, 20°C, 35°C, and 50°C), the setup was placed in a refrigerator, at room temperature, and in two ovens (see Figure 2c). After completion of the biological treatment process for the soils in the columns, the specimens were flushed with two pore volumes of deionized water to eliminate all excess soluble salts before removing the specimens from the columns following established practices (Whiffin et al. 2007; Dejong et al. 2010).

2.4 Triaxial tests

Consolidated drained (CD) triaxial tests (ASTM 2020) were conducted to determine the strength and stress-strain relationships of MICP-treated specimens. In the study by Montoya and DeJong (2015) on MICP-treated sands, samples were prepared by first applying confining pressure, followed by MICP treatment to match field soil conditions. However, in other studies such as Cui et al. (2017) and Gao et al. (2018), samples were treated with MICP first, demolded, and then positioned in the test apparatus before applying confining pressures for triaxial tests. Due to temperature requirements, the procedure of Cui et al. (2017) and Gao et al. (2018) was followed in this study. It should be noted that this procedure may damage some cementation bonds before triaxial shear begins, potentially resulting in lower strength parameters than the true values.

First, the specimens were saturated with deionized water using a vacuum saturation method for 24 hours and then placed in the triaxial apparatus. Hydraulic saturation was applied for 12 hours at a confining pressure of 20 kPa, and back-pressure saturation was sequentially applied until the Bvalue exceeded 0.95. After consolidation, the confining pressure was maintained, and the specimens were sheared under drained conditions at a constant displacement loading rate of 0.1 mm/min. Stress-strain curves were obtained for each confining pressure to determine peak and residual strength, with the residual strength defined as the stress level at which the yield strength stabilized after a decrease from the peak strength due to accumulated damage (at a strain of 20% in this case). The two key shear strength parameters, friction angle and cohesion strength, were obtained by consolidating each of the four samples at effective confining pressures of 100, 200, 300, and 400 kPa based on the Mohr-Coulomb (MC) failure criterion (Wood 1990).

2.5 $CaCO_3$ content measurement and chemical efficiency calculation

After completion of the triaxial tests, samples weighing between 15 to 25 g were collected every 15 mm along the height of the sand column. These samples were subjected to oven-drying at 105°C for at least 24 hours to determine their $CaCO_3$ content using the ASTM Method (ASTM 2014). To perform the measurement, each sample was mixed with 30 ml of 3 M hydrochloric acid inside a sealed chamber, ensuring no contact between samples. The chamber was gently agitated to allow for the reaction between $CaCO_3$ and hydrochloric acid, which produced CO_2, leading to an increase in pressure within the chamber. The reading was taken when the pressure gauge indicated no further change in pressure, and the amount of $CaCO_3$ was calculated as follows:

$$CaCO_3(g) = 0.034 \cdot CO_2 \text{ pressure} + 0.0198 \tag{3}$$

The chemical conversion efficiency of MICP was then calculated, which is defined as the ratio of the precipitated mass of $CaCO_3$ in the sand to the calculated mass of $CaCO_3$ from cementation solutions (Wang 2018):

$$Efficiency(\%) = \frac{m(\text{CaCO}_3)/m_1(\text{sand})}{c(\text{CaCl}_2)\cdot V \cdot M(\text{CaCO}_3)/m_2(\text{sand})} \times 100\% \quad (4)$$

where, *m(CaCO₃)/m₁(sand)* is the measured $CaCO_3$ content, *c(CaCl₂)* is the concentration of $CaCl_2$ in the cementation solutions, *V* is the total volume of cementation solution injected into samples, *M(CaCO₃)* is the molar mass of $CaCO_3$ (100 g/mol), and *m₂(sand)* is the dry mass of sand used to prepare sample columns.

2.6 Scanning electron microscopy (SEM) imaging and X-ray diffraction (XRD) analyses

After the MICP treatment, samples were oven-dried at 105°C and prepared for scanning electron microscopy (SEM) imaging using a PHENOM XL Scanning Electron Microscope to investigate the microscale properties of the $CaCO_3$ crystals that formed. Additionally, X-ray diffraction (XRD) analysis was performed on the samples treated at different temperatures using a Regiku Miniflex 600 X-ray diffractometer.

3 Results and discussion

3.1 $CaCO_3$ content and chemical efficiency

In the case of a single bacterial suspension injection (Fig. 3a), the highest average $CaCO_3$ content was obtained at 35°C (sample T35(BS1) in Fig. 3a), while temperatures of 4°C and 50°C resulted in relatively lower average $CaCO_3$ contents (samples T4(BS1) and T50(BS1) in Fig. 3a). Injecting bacterial suspension multiple times increases the average $CaCO_3$ content (Fig. 3b). The distribution of $CaCO_3$ content along the height of the sand column becomes more heterogeneous as the average $CaCO_3$ content increases (Fig. 3a and b). Least-squares regression was used to obtain the fit lines of the data. The chemical conversion efficiency of the sample ranges from 17.3% to 67%, with the peak obtained at 35°C (Fig. 3c). At 50°C, the chemical conversion efficiency is logarithmically fitted with the number of BS injections, ranging from 17.3% to 56.5% (Fig. 3d).

The findings of this study are consistent with those of Wang et al. (2022b), except for the highest $CaCO_3$ content, which was achieved at 35°Cin this study, while Wang et al. (2022b) reported the highest content at 20°C. The difference may be attributed to the variation in the interval between consecutive injections of the cementation solution in the two studies. Wang et al. (2022b) used a 48-hour interval, while this study employed a 24-hour interval, which was sufficient to precipitate 0.5 M of CS at both 20°C and 35°C. As bacterial activity decreases over time at higher temperatures, the shorter injection interval maintained a relatively higher bacterial activity and $CaCO_3$ conversion efficiency, indicating that the injection interval between BS and CS needs to be carefully considered at higher temperatures (e.g., 50°C). Moreover, increasing the number of BS injections compensated for bacterial decay caused by high temperature, maintained the supersaturation state in the solution, and resulted in higher $CaCO_3$ content than the amount produced when BS was injected only once. Therefore, a 24-hour injection interval is suitable for temperatures below 35°C, while a shorter interval should be adopted at high-temperature conditions to ensure the desired treatment effect.

3.2 Stress-strain and volumetric-strain responses

Previous studies by Feng and Montoya (2016) and Xiao et al. (2019) have shown that samples treated with microbial-induced calcium carbonate precipitation (MICP) at room temperature exhibit strain softening behavior. This study confirms that strain softening is not dependent on treatment temperature, as samples treated at temperatures ranging from 4 to 50°C showed similar behavior. However, more pronounced softening was observed at 20°C and 35°C, while gradual softening was observed at 4°C and 50°C after reaching peak strength (Fig. 4). Peak strength increased with increasing confining pressure, as expected. At 50°C, an increase in the number of injections of bacterial suspension resulted in increased peak strength and brittle behavior of the samples (Fig. 4).

All MICP-treated samples exhibited volumetric expansion at small strains and a dilative response at large strain (Fig. 5). The amount of dilation decreased with increasing confining pressures (Fig. 5 a-d). Samples treated at 4°C and 50°C exhibited less contraction at small strains compared to those treated at 20°C and 35°C. Among all temperatures, the sample treated at 35°C showed the largest dilatancy when the strain was 15% at a given confining pressure (e.g., 100 kPa), followed by those treated at 20°C, 4°C, and 50°C (Fig. 5a). The volumetric behavior of the samples was related to the treatment temperature, which directly affects the $CaCO_3$ content. Higher carbonate content led to higher dilatancy at large strains at a given confining pressure, as reported by other studies (e.g., Lin et al., 2016; Xiao et al., 2019) conducted at room temperature. When the strain was small, contraction was observed for all samples, but samples treated at 50°C showed substantial dilatancy improvement as the number of injections of bacterial suspension was increased.

The stress paths and critical state lines in q-p' space are shown in Fig. 6 (a) and (b). The critical state lines moved upwards with increasing $CaCO_3$ content produced in samples at varied temperatures or with varying numbers of bacterial injections. This indicates that temperature and bacterial injection number influence the $CaCO_3$ content produced, which consequently affects the strength behavior of

MICP-treated soil. The low strength behavior of MICP-treated soil at 50°C can be improved by increasing the number of injections of bacterial suspension.

3.3 Peak strength and residual strength

The increase in confining pressure led to an increase in both peak strength (q_p) and residual strength (q_R), as shown in Fig. 7 b and d. For instance, the peak strength of the sample treated at 20°C rose from 623.6 kPa to 1576.8 kPa as the confining pressure was increased from 100 kPa to 400 kPa, while the residual strength rose from 271.7 kPa to 812.2 kPa (Fig. 7). Increasing the number of BS injections also resulted in a important improvement in both peak and residual strengths (Fig. 7 b and d).

The effect of temperature and number of BS injections on peak and residual strengths can be attributed to the variation in $CaCO_3$ content, as illustrated in Fig. 7 by the $CaCO_3$ contents. In the residual state, the strength of the sample is mainly due to the non-broken calcium carbonate between particles and the surface roughness of soil particles caused by $CaCO_3$ precipitation. The cementation degraded substantially after reaching the peak state, especially in stronger specimens, but the non-broken calcite still acts as cementation, and the roughness of sand particles may also contribute to the residual strength.

Multiple BS injections resulted in an increase in peak and residual strengths because the calcite crystal clusters grew in size. However, the sample with the highest strength was still the one with one injection of BS at 35°C. This highlights the significance of adjusting the temperature specifically for each MICP application. In cases where temperature cannot be controlled, altering the MICP recipe, specifically the number of bacterial solution injections, is suggested.

3.4 Effective strength parameters

Fig. 8a shows that the effective cohesion and friction angle of the sand sample initially increased and then decreased as the temperature increased from 4°C to 50°C. The effective strength parameters were smaller at lower and higher temperatures compared to those in the temperature range of 4°C-50°C. Within this range, the effective cohesion and friction angle varied from 3.1 kPa to 80.9 kPa and from 26.8° to 36.6°, respectively. The effective cohesion and friction angle increased linearly with an increase in the number of bacterial solution injections. Furthermore, the effective cohesion increased exponentially with an increase in the average $CaCO_3$ content, while the effective friction angle increased linearly with the average $CaCO_3$ content, as depicted in Figure 9. These results are consistent with previous studies conducted at a standard temperature of 25°C (e.g., Cui et al. 2017; Chou et al. 2020).

Temperature has a noteworthy effect on the strength of sand treated with MICP, with $CaCO_3$ content and product uniformity being the primary factors (Feng and Montoya 2016; Cui et al. 2017; Nafisi et al. 2020; Konstantinou et al. 2021). Previous triaxial testing studies have shown that an increase in $CaCO_3$ content leads to an increase in both effective cohesion and friction angle (Cui et al. 2017; Chou et al. 2020). For non-cemented soil, grain size distribution, angularity, and particle interlocking primarily affect the effective cohesion and friction angle. However, for cemented soil, $CaCO_3$ precipitation has a bonding effect on sand cementation, leading to a substantial increase in cohesion, which defines the non-frictional part of shear resistance (DeJong et al. 2010). Additionally, the ‘added’ calcium carbonate crystals increase particle interlocking, leading to an increase in the friction angle. The study shows that the increase in cohesion is more pronounced than the increase in friction angle in MICP-treated specimens due to the added cementation at the contact points.

3.5 Microstructure characterization

As the temperature increased from 4°C to 35°C, more $CaCO_3$ crystals precipitated on the surface of sand particles or at the particle contacts. However, for the sample treated at 50°C, the number of $CaCO_3$ crystals decreased dramatically. This is consistent with the macro-scale measurement of $CaCO_3$ content shown in Figure 3. The size of the $CaCO_3$ crystals also varied with temperature. Small crystals mainly precipitated in samples treated at 4°C, while larger crystal clusters were formed in samples treated at 20°C and 35°C. On the other hand, crystal clusters were observed at 50°C, but their size was smaller than those obtained at 20°C and 35°C. The size of the crystal clusters increased with the increase in the number of BS injections, with the average diameter of crystal clusters reaching 25 μm and 40 μm for samples treated with BS injected 3 times and 6 times, respectively (Figure 10).

The XRD diagrams confirmed the presence of calcite at the peaks with angles of 29.4° and 55° (Figure 11). To further analyze the data, the areas under the two peaks were measured for each condition and presented in Table 2 (units in cps*degrees). The findings showed that the optimum point was at 35 degrees Celsius, where both areas under the two peaks were larger. The carbonate measurements with the acid method also supported these results as shown previously.

3.6 Correlation between $CaCO_3$ microstructure and soil strength behavior

Figure 12 illustrates magnified SEM images (Figure 12a) and a schematic of cementing pattern (Figure 12b). The distinguish of crystal cluster is also illustrated in Figure 12a. At 20℃, 35℃, and 50℃, smaller and more crystals form into clusters in the cementing pattern (compared to the case with multiple BS injections), whereas at 4℃, the cluster pattern is not evident. Increasing the number of BS injections at 50℃ results in larger crystals. Figure 13 presents the quantification of number and size of crystal or clusters, with crystal or clusters numbered according to size. Among the four temperatures (4℃, 20℃, 35℃, and 50℃), 20℃ (see Figure 12 and Figure 13b) produces the largest crystal number range, while 35℃ produces the largest crystal size range (see Figure 12 and Figure 13c). This indicates that 4℃ and 50℃ produce fewer and smaller crystals, while 20℃ and 35℃ produce more and larger crystal clusters. Moreover, 20℃ produces a larger number of smaller clusters than 35℃ (see Figure 12 and Figure 13 b-c). In the case of multiple bacterial injections, larger crystals tend to form instead of forming large clusters (See Figure 12). The size of crystal increases as the number of BS injections increases from 1 to 6 (Figure 13d-f). This might be because the injected bacteria preferentially attach to calcite, which acts as a better nucleation site for crystals than quartz.

Based on Figures 12 and 13, it can be concluded that when bacteria are only injected once, but the temperature changes, clusters with different sizes and numbers tend to form with temperature changes. However, when the temperature is fixed at 50℃, but the injection number of bacterial suspension increases, large crystals tend to form. To compare the effect of clusters and larger crystals on increasing the strength behavior of MICP treatment, the correlation between average $CaCO_3$ and effective cohesion, effective friction angle, peak deviatoric stress, and residual deviatoric stress were analyzed separately for tests 1-4 and 4-6 (results are shown in Figures 14 and 15).

The results indicate that when the $CaCO_3$ content is the same, compared to large $CaCO_3$, crystal clusters are more effective in increasing effective cohesion (Figure 14a), peak strength (Figure 15), and residual strength (Figure 15). This may be because increasing cluster size not only improves bonding efficiency, leading to an increase in cohesion but also enhances surface roughness, resulting in a more effective increase in friction. However, large crystals are more effective in increasing the effective friction angle at the low average $CaCO_3$ content range compared to crystal clusters and less effective at the high average $CaCO_3$ content range. This may be because, at the low average $CaCO_3$ content range, the big crystals are more effective in forming friction between soil particles, compared to smaller but a larger number of crystals. However, at the high average $CaCO_3$ content range, the big crystals are still effective in forming friction between soil particles, but because the crystals are big, the number of crystals is fewer compared to crystal clusters, resulting in reduced overall friction effectiveness. Further work can be done to study the effect of crystal and cluster properties on MICP-treated soil, both experimentally and numerically.

4 Conclusions

This study aimed to investigate the effectiveness of microbially induced calcium carbonate precipitation (MICP) in treating granular media at different temperatures. A series of consolidated drained triaxial compression tests were conducted to evaluate the engineering properties of treated soils, and micro-scale investigation was conducted to explore the characteristics of the precipitated minerals responsible for these properties. Based on the findings, the following conclusions were drawn:

Increasing the treatment temperature from 4°C to 35°C increased the CaCO3 content of samples, but at 50°C, the content decreased considerably. All MICP-treated samples exhibited strain softening and volumetric dilatancy, with peak and residual strength values varying with treatment temperature. Samples treated at 35°C exhibited the highest peak and residual strength, followed by 20°C, while samples treated at lower and higher temperatures resulted in lower strength. Increasing the number of bacterial solution injections improved the peak and residual strength of samples treated at 50°C.

The effective cohesion and friction angle followed a similar pattern as peak and residual strength, increasing and then decreasing with temperature. The amount of CaCO3 precipitation was attributed to the difference in strength enhancement of MICP-treated sand at different temperatures.

SEM images and XRD results showed that rhombohedral calcite was the dominant type of CaCO3 crystals produced at different temperatures, with most crystals forming as clusters on particle surfaces or at particle contacts. Crystal cluster sizes increased as the temperature increased from 4°C to 35°C and decreased at 50°C.

The mechanical behavior of MICP-treated sand was found to be closely related to treatment temperature, and altering the MICP recipe, specifically the number of bacterial solution injections, was suggested as a potential solution when temperature cannot be controlled. The efficiency of MICP in soil strength enhancement was found to depend on the properties of produced CaCO3, and any environmental factors affecting these properties should be considered when predicting MICP efficiencies.

The study showed that crystal clusters are better than large crystals in increasing effective cohesion, peak strength, and residual strength when CaCO3 content is the same, due to improved bonding efficiency and surface roughness. However, large crystals are more effective in increasing the effective friction angle at low average $CaCO_3$ content range. Further research is needed to explore the impact of crystal and cluster properties on MICP-treated soil.

Data Availability Statement

Some or all data, models, or code that support the findings of this study are available from the corresponding author upon reasonable request.

Acknowledgements

Y.W. acknowledges the financial support of National Natural Science Foundation of China (Grant No. 52171262); Science, Technology and Innovation Commission of Shenzhen Municipality (Grant No. JCYJ20210324103812033, ZDSYS20200421111201738) for conducting this study.

References

1. ASTM (2014). Standard test method for rapid determination of carbonate content of soils.

ASTM D4373-14. West Conshohocken, PA.

2. ASTM (2017). Standard Practice for Classification of Soils for Engineering Purposes (Unified Soil Classification System). ASTM D2487−17. West Conshohocken, PA.
3. ASTM (2020). Standard Test Method for Consolidated Drained Triaxial Compression Test for Soils. ASTM D7181-20. West Conshohocken, PA.
4. Burghignoli, A., Desideri, A., & Miliziano, S. (2000). A laboratory study on the thermomechanical behaviour of clayey soils. Canadian Geotechnical Journal, 37(4), 764-780.
5. Cheng, L., Shahin, M. A., & Mujah, D. (2017). Influence of key environmental conditions on microbially induced cementation for soil stabilization. Journal of Geotechnical and Geoenvironmental Engineering, 143(1), 04016083.
6. Chek, A., Crowley, R., Ellis, T. N., Durnin, M., & Wingender, B. (2021). Evaluation of factors affecting erodibility improvement for MICP-treated beach sand. Journal of Geotechnical and Geoenvironmental Engineering, 147(3), 04021001.
7. Chou, Sun-Gyu, Chang, Ilhan, Lee, Minhyeong, Lee, Ju-Hyung, Han, Jin-Tae, Kwon, Tae-Hyuk. 2020. Review on geotechnical engineering properties of sands treated by microbially induced calcium carbonate precipitation (MICP) and biopolymers. Construction and Building Materials, 246: 118415.
8. Cui, M. J., Zheng, J. J., Zhang, R. J., Lai, H. J., & Zhang, J. (2017). Influence of cementation level on the strength behaviour of bio-cemented sand. Acta Geotechnica, 12(5), 971-986.
9. Cuthbert M.O., McMillan L.A., Handley-Sidhu S., Riley M.S., Tobler D.J., Phoenix V.R., A field and modeling study of fractured rock permeability reduction using microbially induced calcite precipitation, Environ. Sci. Technol. 47 (23) (2013) 13637–13643, https://doi.org/10.1021/es402601g

10. Darby, Kathleen M., Hernandez, Gabby L., DeJong, Jason T., Boulanger, Ross W., Gomez, Michael G., Wilson, Daniel W. (2019). Centrifuge Model Testing of Liquefaction Mitigation via Microbially Induced Calcite Precipitation. Journal of Geotechnical and Geoenvironmental Engineering, 145, 10: 04019084.

11. DeJong, J. T., Fritzges, M. B., & Nüsslein, K. (2006). Microbially induced cementation to control sand response to undrained shear. Journal of Geotechnical and Geoenvironmental Engineering, 132(11), 1381-1392.

12. DeJong, J. T., Mortensen, B. M., Martinez, B. C., & Nelson, D. C. (2010). Bio-mediated soil improvement. Ecological Engineering, 36(2), 197-210.

13. Feng, K., & Montoya, B. M. (2016). Influence of confinement and cementation level on the behavior of microbial-induced calcite precipitated sands under monotonic drained loading. Journal of Geotechnical and Geoenvironmental Engineering, 142(1), 04015057. DOI: 10.1061/(ASCE)GT.1943-5606.0001379.

14. Fujii, T., Suzuki, K., Takayama, T., Tamaki, M., Komatsu, Y., Konno, Y., Yoneda, J., Yamamoto, K. and Nagao, J. 2015. Geological setting and characterization of a methane hydrate reservoir distributed at the first offshore production test site on the Daini-Atsumi Knoll in the eastern Nankai Trough, Japan. Mar. Pet. Geol. 66, 310-322.

15. Gao Y., Hang L., He J., Chu J. (2018). Mechanical behaviour of biocemented sands at various treatment levels and relative densities, Acta Geotech 14 (3), 697–707, https://doi.org/10.1007/s11440-018-0729-3

16. Gomez, M. G., Anderson, C. M., Graddy, C. M., DeJong, J. T., Nelson, D. C., & Ginn, T. R. (2017). Large-scale comparison of bioaugmentation and biostimulation approaches for

biocementation of sands. Journal of geotechnical and geoenvironmental engineering, 143(5), 04016124.

17. Graddy, C. M., Gomez, M. G., DeJong, J. T., & Nelson, D. C. (2021). Native bacterial community convergence in augmented and stimulated ureolytic MICP biocementation. Environmental Science & Technology, 55(15), 10784-10793.

18. Guo Z., Wang W., Guo N., Zeng Z., Liu T., Wang X., Molybdenum-mediated chemotaxis of Pseudoalteromonas lipolytica enhances biofilm-induced mineralization on low alloy steel surface, Corros. Sci. (2019) 159, https://doi.org/10.1016/j.corsci.2019.108123

19. Hata, T., Saracho, A. C., Haigh, S. K., Yoneda, J., & Yamamoto, K. (2020). Microbial-induced carbonate precipitation applicability with the methane hydrate-bearing layer microbe. Journal of Natural Gas Science and Engineering, 81, 103490.

20. Jiang, N. J., Soga, K., & Kuo, M. (2017). Microbially induced carbonate precipitation for seepage-induced internal erosion control in sand–clay mixtures. Journal of Geotechnical and Geoenvironmental Engineering, 143(3), 04016100.

21. Jing J., Shan H., Zhu X., Huangpu Y. and Tian Y. Wellbore Temperature and Pressure Calculation of Offshore Gas Well Based on Gas–Liquid Separated Flow Model. Processes, 2022, 10, 2043. https://doi.org/10.3390/pr10102043

22. Konstantinou, C., Biscontin, G., Jiang, N. J., & Soga, K. (2021a). Application of microbially induced carbonate precipitation to form bio-cemented artificial sandstone. Journal of Rock Mechanics and Geotechnical Engineering, 13(3), 579-592.

23. Konstantinou, C., Wang, Y., Biscontin, G., & Soga, K. (2021b). The role of bacterial urease activity on the uniformity of carbonate precipitation profiles of bio-treated coarse sand

specimens. Scientific reports, 11(1), 1-17.

24. Li, J.-f., Ye, J.-l., Qin, X.-w., Qiu, H.-j., Wu, N.-y., Lu, H.-l., Xie, W.-w., Lu, J.-a., Peng, F. and Xu, Z.-q. 2018. The first offshore natural gas hydrate production test in South China Sea. China geology 1(1), 5-16.

25. Lin, H., Suleiman, M. T., Brown, D. G., & Kavazanjian Jr, E. (2016a). Mechanical behavior of sands treated by microbially induced carbonate precipitation. Journal of Geotechnical and Geoenvironmental Engineering, 142(2), 04015066.

26. Lin H., Suleiman M.T., Jabbour H. M., Brown D. G., Kavazanjian Jr. E. (2016b). Enhancing the Axial Compression Response of Pervious Concrete Ground Improvement Piles Using Biogrouting, J. Geotech. Geoenviron. Eng., 142(10): 04016045

27. Lin H., O'Donnell S. T., Suleiman M.T., Kavazanjian Jr. E., and Brown D. G. (2021). Effects of Enzyme and Microbially Induced Carbonate Precipitation Treatments on the Response of Axially Loaded Pervious Concrete Piles, J. Geotech. Geoenviron. Eng., 147(8): 04021057

28. Lioliou, M. G., Paraskeva, C. A., Koutsoukos, P. G., & Payatakes, A. C. (2007). Heterogeneous nucleation and growth of calcium carbonate on calcite and quartz. Journal of colloid and interface science, 308(2), 421-428.

29. Liu H., Liu H. Xiao Y., McCartney J.S. (2018). Effects of temperature on the shear strength of saturated sand, Soils and Foundations 58: 1326–1338

30. Martinez, B. C., DeJong, J. T., Ginn, T. R., Montoya, B. M., Barkouki, T. H., Hunt, C., Tanyu, B., Major, D. (2013). Experimental Optimization of Microbial-Induced Carbonate Precipitation for Soil Improvement. Journal of Geotechnical and Geoenvironmental

Engineering, 139(4): 587-598.

31. Martinez A., Huang L., Gomez M.G. (2019).Thermal conductivity of MICP-treated sands at varying degrees of saturation, Géotech. Lett. 9 (1) 15–21, https://doi. org/10.1680/jgele.18.00126

32. Mitchell, J. K., & Santamarina, J. C. (2005). Biological considerations in geotechnical engineering. Journal of geotechnical and geoenvironmental engineering, 131(10), 1222-1233.

33. Montoya, B. M., DeJong, J. T., & Boulanger, R. W. (2013). Dynamic response of liquefiable sand improved by microbial-induced calcite precipitation. Géotechnique, 63, No. 4, 302–312 [http://dx.doi.org/10.1680/geot.SIP13.P.019]

34. Montoya, B. M., & DeJong, J. T. (2015). Stress-strain behavior of sands cemented by microbially induced calcite precipitation. Journal of Geotechnical and Geoenvironmental Engineering, 141(6), 04015019.

35. Nafisi, A., Montoya, B. M., & Evans, T. M. (2020). Shear strength envelopes of biocemented sands with varying particle size and cementation level. Journal of Geotechnical and Geoenvironmental Engineering, 146(3), 04020002.

36. Naveed, Muhammad, Jiangong Duan, Shahab Uddin, Muhammad Suleman, Yang Hui, and Hongyu Li. (2020). Application of Microbially Induced Calcium Carbonate Precipitation with Urea Hydrolysis to Improve the Mechanical Properties of Soil. Ecological Engineering. Elsevier B.V. https://doi.org/10.1016/j.ecoleng.2020.105885.

37. Phillips A.J., Troyer E., Hiebert R., Kirkland C., Gerlach R., Cunningham A.B., Spangler L., Kirksey J., Rowe W., Esposito R., Enhancing wellbore cement integrity with microbially induced calcite precipitation (MICP): a field scale demonstration, Journal of Petroleum Science and Engineering 171 (2018) 1141–1148, https://doi.org/10.1016/j.petrol.2018.08.012

38. Tang S., Sun S., Liu T., Li M., Jiang Y., Wang D., Guo N., Guo Z., Chang X., Bionic engineering-induced formation of hierarchical structured minerals with superwetting surfaces for oil-water separation, J. Membr. Sci. (2023) 669, https://doi. org/10.1016/j.memsci.2022.121261

39. Tian, Z., Shi, L., & Qiao, L. (2015). Problems in the wellbore integrity of a shale gas horizontal well and corresponding countermeasures. Natural Gas Industry B, 2(6), 522-529.

40. Toribio M.M., Oshima Y. and Shimada S. (2004). Evaluation of Sequesterable Carbon Dioxide in Japanese Coal Samples at Sub-critical and Supercritical Conditions. Studies in Surface Science and Catalysis 153. 375-380

41. Tobler, Dominique J., James M. Minto, Gráinne el Mountassir, Rebecca J. Lunn, and Vernon R. Phoenix. (2018). Microscale Analysis of Fractured Rock Sealed With Microbially Induced CaCO3 Precipitation: Influence on Hydraulic and Mechanical Performance. Water Resources Research 54 (10): 8295–8308. https://doi.org/10.1029/2018WR023032.

42. van Paassen, L. A., Ghose, Ranajit, van der Linden Thomas, J. M., van der Star Wouter, R. L., van Loosdrecht Mark, C. M. (2010). Quantifying Biomediated Ground Improvement by Ureolysis: Large-Scale Biogrout Experiment. Journal of Geotechnical and Geoenvironmental Engineering, 136(2): 1721-1728

43. Venuleo S., Laloui L., Terzis D., Hueckel T., Hassan M., Microbially induced calcite precipitation effect on soil thermal conductivity, Géotechnique Letters 6 (1) (2016) 39–44, https://doi.org/10.1680/jgele.15.00125

44. Wang Y. (2018). Microbial-Induced Calcium Carbonate Precipitation: from Micro to Macro

Scale. Ph.D. thesis, University of Cambridge, United Kingdom.

45. Wang, Y., Soga, K., DeJong, J. T., & Kabla, A. J. (2021). Effects of Bacterial Density on Growth Rate and Characteristics of Microbial-Induced $CaCO_3$ Precipitates: Particle-Scale Experimental Study. Journal of Geotechnical and Geoenvironmental Engineering, 147(6), 04021036.

46. Wang, Y., Konstantinou C., Soga K., Biscontin G., Kabla A. J., Y. (2022). Use of microfluidic experiments to optimize MICP treatment protocols for effective strength enhancement of MICP-treated sandy soils. Acta Geotechnica, 1-22.

47. Wang, Y., Wang, Y., Soga, K. et al. Microscale investigations of temperature-dependent microbially induced carbonate precipitation (MICP) in the temperature range 4–50 °C. Acta Geotech. 18, 2239–2261 (2023). https://doi.org/10.1007/s11440-022-01664-9

48. Wang, Y., Konstantinou, C., Tang, S., & Chen, H. (2023). Applications of microbial-induced carbonate precipitation: A state-of-the-art review. Biogeotechnics, 100008.

49. Whiffin V.S., van Paassen L.A., Harkes M.P., Microbial carbonate precipitation as a soil improvement technique, Geomicrobiol. J. 24 (5) (2007) 417–423, https://doi. org/10.1080/01490450701436505

50. Xiao, Peng, Liu, Hanlong, Xiao, Yang, Stuedlein, Armin W., Evans, T. Matthew (2018). Liquefaction resistance of bio-cemented calcareous sand. Soil Dynamics and Earthquake Engineering, 107: 9-19.

51. Xiao Y., Wang Y., Desai C.S., Jiang X., Liu H. (2019). Strength and deformation responses of biocemented sands using a temperature-controlled method, Int. J. Geomech 19 (11), https://doi.org/10.1061/(asce)gm.1943-5622.0001497

52. Xiao, Y., Zhao, C., Sun, Y., Wang, S., Wu, H., Chen, H., & Liu, H. (2021). Compression behavior of MICP-treated sand with various gradations. Acta Geotechnica, 16(5), 1391-1400.

53. Ye, J.-l., Qin, X.-w., Xie, W.-w., Lu, H.-l., Ma, B.-j., Qiu, H.-j., Liang, J.-q., Lu, J.-a., Kuang, Z.-g. and Lu, C. 2020. The second natural gas hydrate production test in the South China Sea. China Geology 3(2), 197-209.

54. Zamani, A., Montoya, B. M., & Gabr, M. A. (2019). Investigating challenges of in situ delivery of microbial-induced calcium carbonate precipitation (MICP) in fine-grain sands and silty sand. Canadian Geotechnical Journal, 56(12), 1889-1900.

55. Zamani A.; Xiao P.; Baumer T.; Carey T. J.; Sawyer B.; DeJong J. T.; and Boulanger R.W. (2021). Mitigation of Liquefaction Triggering and Foundation Settlement by MICP Treatment, J. Geotech. Geoenviron. Eng., 147(10): 04021099

56. Zhang C., Shi T., Liu J., He Z., Thomas H., Dong H., Rinkevich B., Wang Y., Hyun J.H., Weinbauer M., Lopez-Abbate C., Tu Q., Xie S., Yamashita Y., Tishchenko P., Chen Q., Zhang R., Jiao N., (2022). Eco-engineering approaches for ocean negative carbon emission, Sci Bull 67 (24) 2564–2573, https://doi.org/10. 1016/j.scib.2022.11.016

Table 1 MICP treatment protocols

Test No.	Sample numbers	Dry density, ρ_d (g/cm^3)	Relative density, D_r (%)	Treating temperature (℃)	Injection number of bacterial suspension	Mean effective stress, p'(kPa)
T4	6	1.48	50	4	1	100, 200, 300, 400
T20	6	1.49	50	20	1	100, 200, 300, 400
T35	6	1.48	50	35	1	100, 200, 300, 400
T50 (BS1)	6	1.48	50	50	1	100, 200, 300, 400
T50 (BS3)	6	1.49	50	50	3	100, 200, 300, 400
T50 (BS6)	6	1.48	50	50	6	100, 200, 300, 400

Table 2 The areas under the two calcite peaks in the XRD diagrams for the various treatment temperature conditions (units in cps*degrees)

	29.4°	**55°**
T4	150.825	180.325
T20	650.975	181.3
T35	806.8	184.225
T50-BS1	51.65	157.225
T50-BS3	107.725	160.325
T50-BS6	115.725	171.3

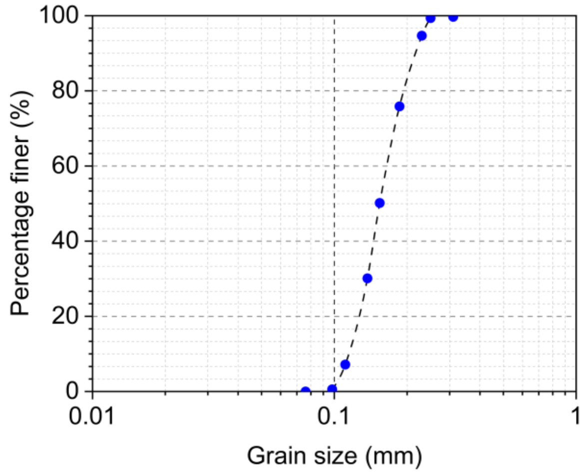

Figure 1 Particle size distribution of the sand used in this study

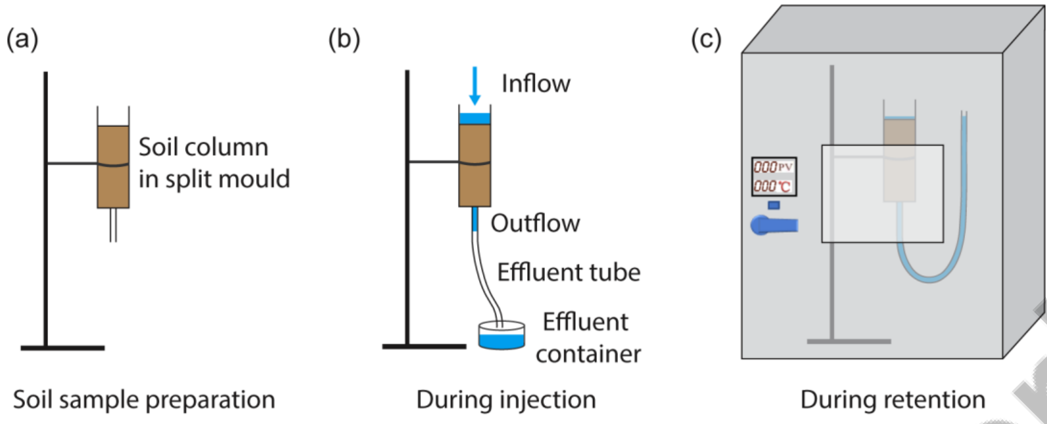

Figure 2 Schematic of the soil column experiments: (a) sand column preparation, (b) and (c) MICP treatment

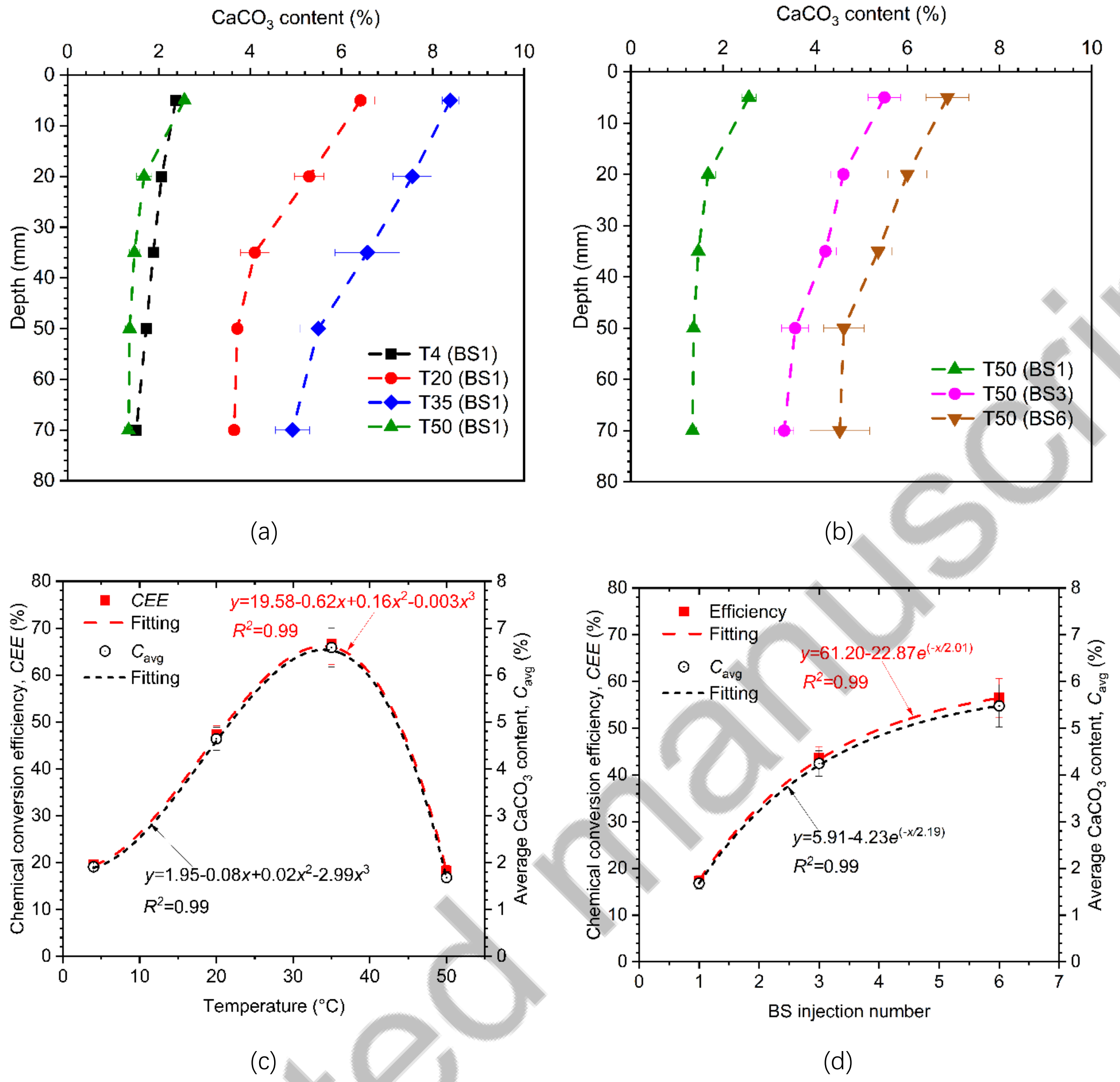

Figure 3 $CaCO_3$ distribution along sand columns and chemical transform efficiency of MICP: (a, c) specimens treated at different temperatures with bacteria introduced only once; (b, d) specimens treated at 50°C with bacteria introduced once, twice, and three times, respectively.

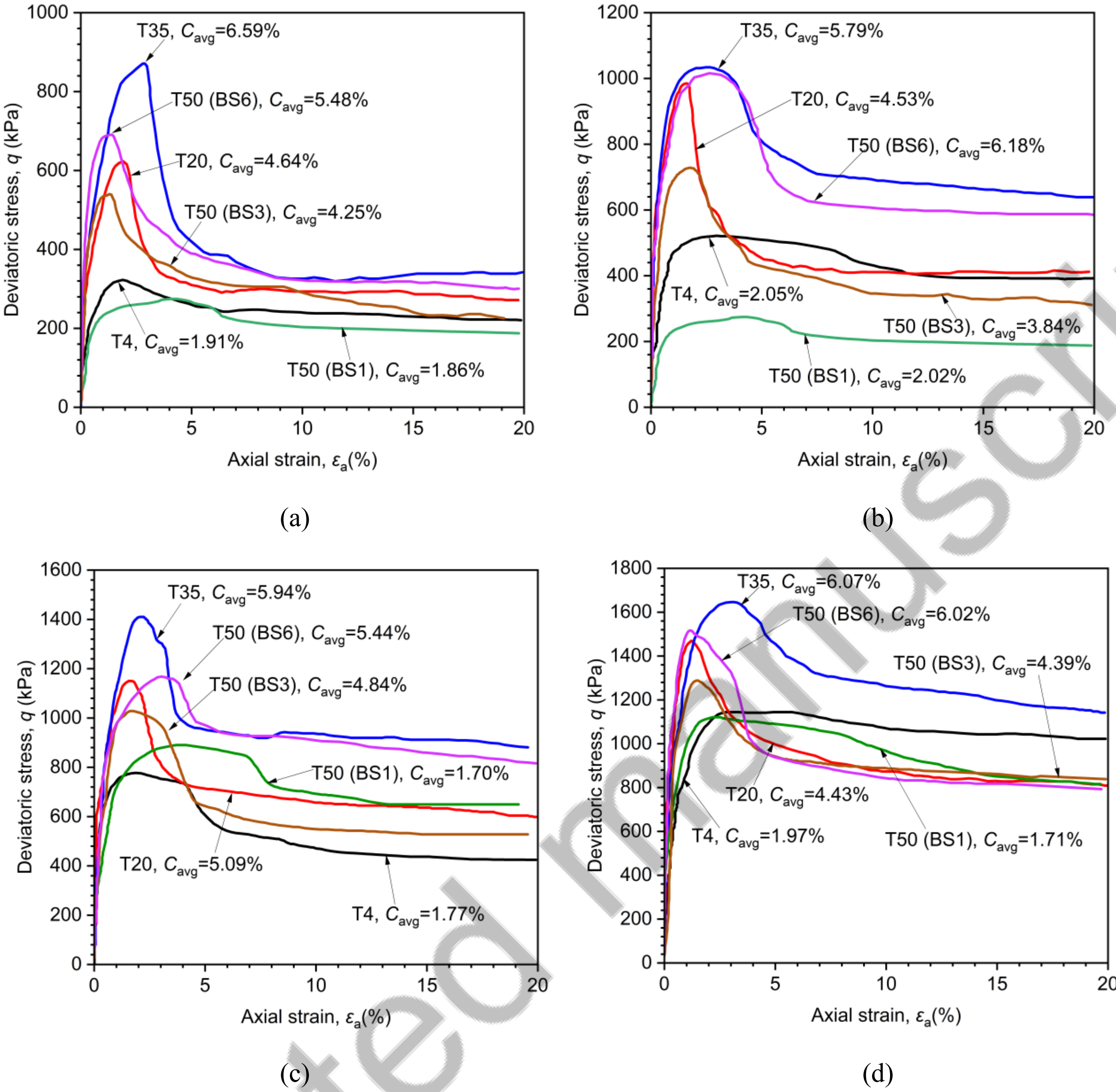

Figure 4 Stress-strain behaviour of MICP-treated sand at different confining pressures: (a) p_c'=100 kPa; (b) p_c'=200 kPa; (c) p_c'=300 kPa; and (d) p_c'=400 kPa; *T*, indicates the treatment temperature, BS, indicates the injection number of bacterial suspension; C_{avg} indicates the average $CaCO_3$ content

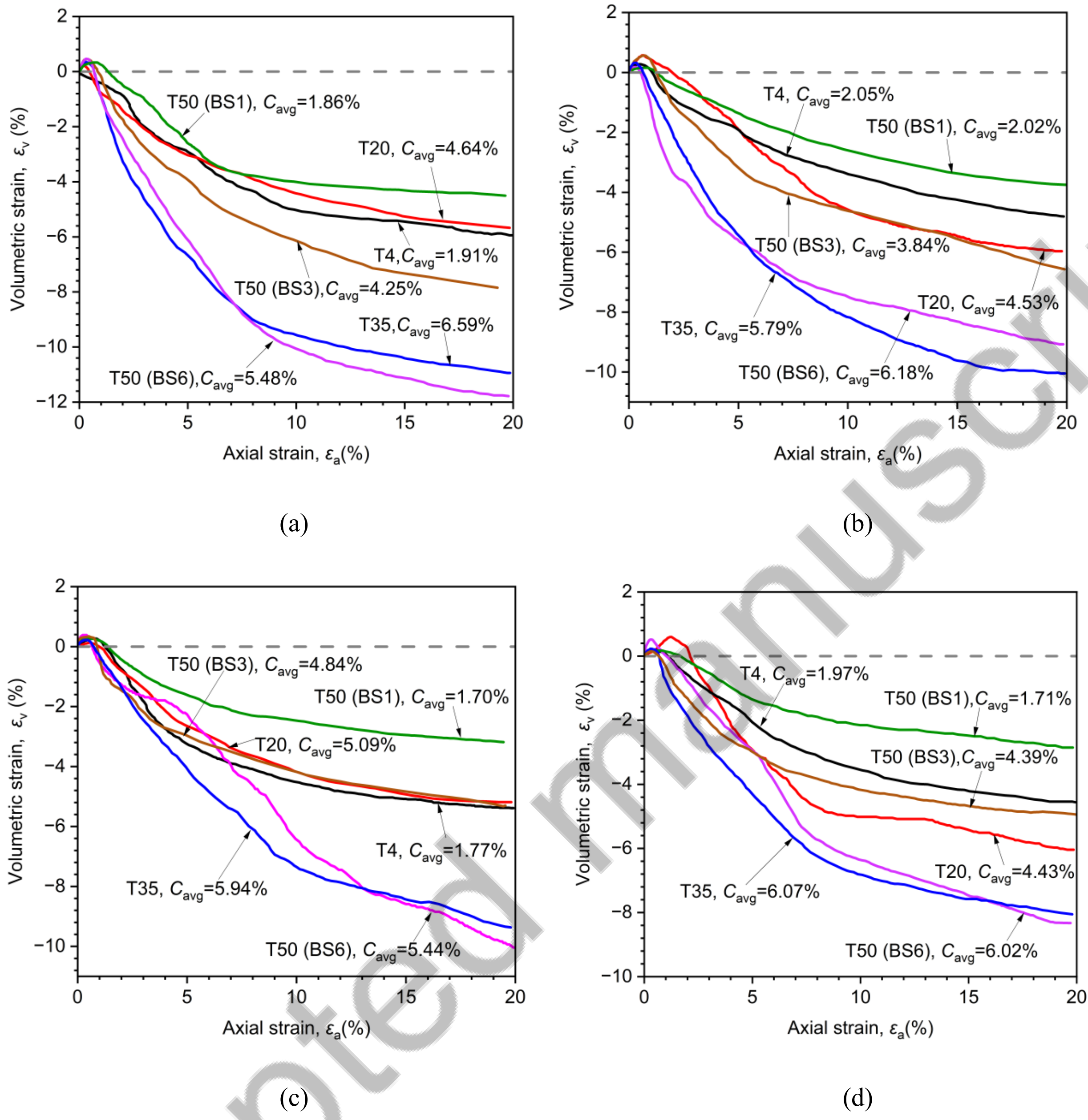

Figure 5 Volumetric behaviour of MICP-treated sand at different confining pressures: (a) p_c'=100 kPa; (b) p_c'=200 kPa; (c) p_c'=300 kPa; and (d) p_c'=400 kPa; *T*, indicates the treatment temperature; BS, indicates the injection number of bacterial suspension; C_{avg} indicates the average $CaCO_3$ content.

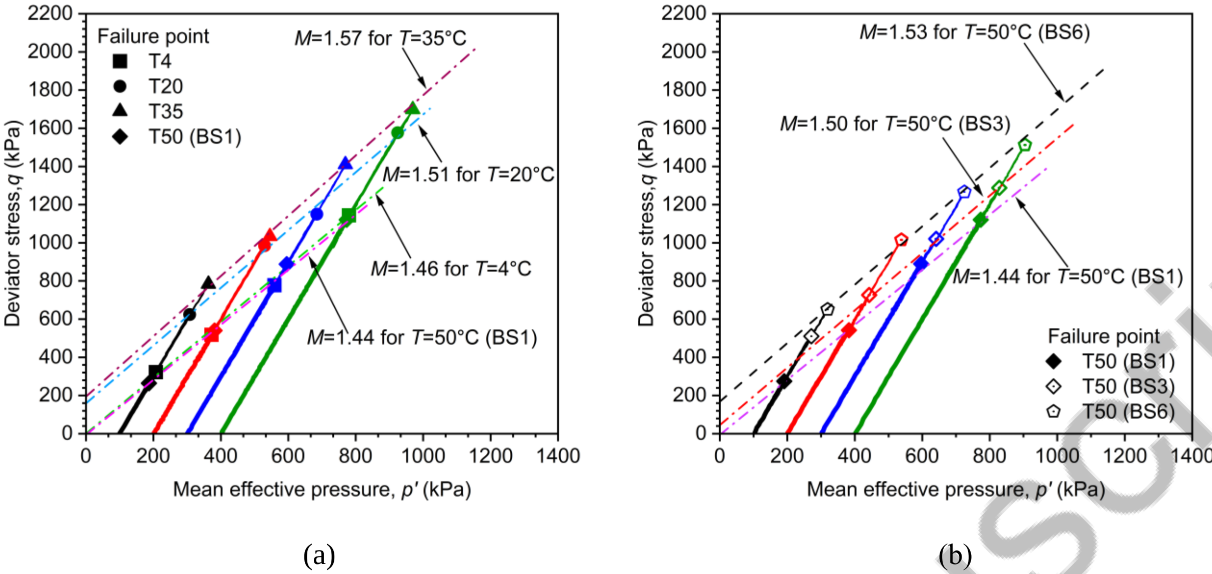

Figure 6 Stress path and critical state line in q-p' space**:** (a) specimens treated at temperatures range from 4℃ to 50℃ with bacteria introduced only once; (b) specimens treated at 50℃ with bacteria introduced once, twice, and three times, respectively.

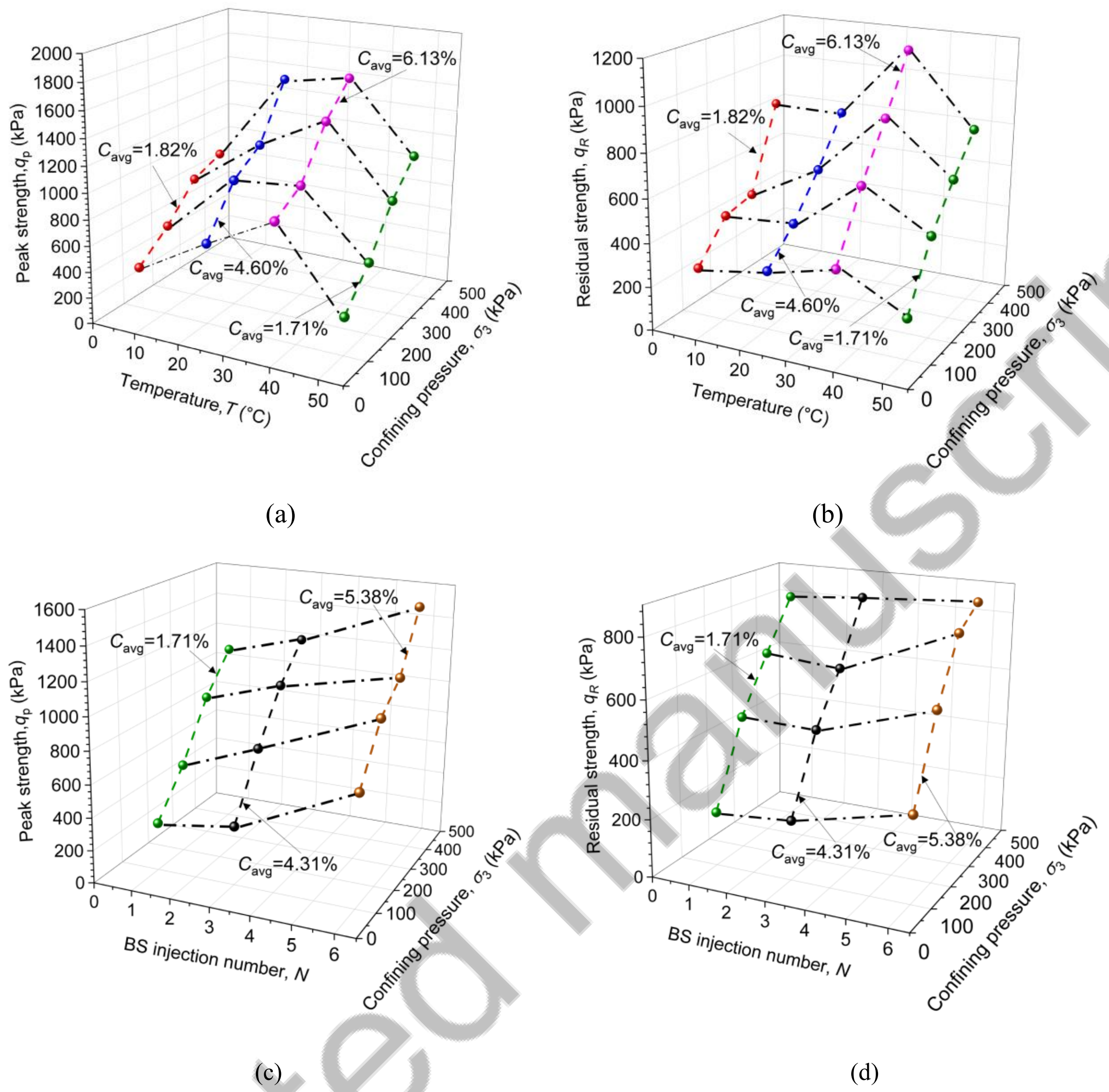

Figure 7 Measured and fitted relationship of q_p-T-σ_3 and q_R-T-σ_3: (a, c) specimens treated at different temperatures with bacteria introduced only once; (b, d) specimens treated at 50°C with bacteria introduced once, twice, and three times, respectively.

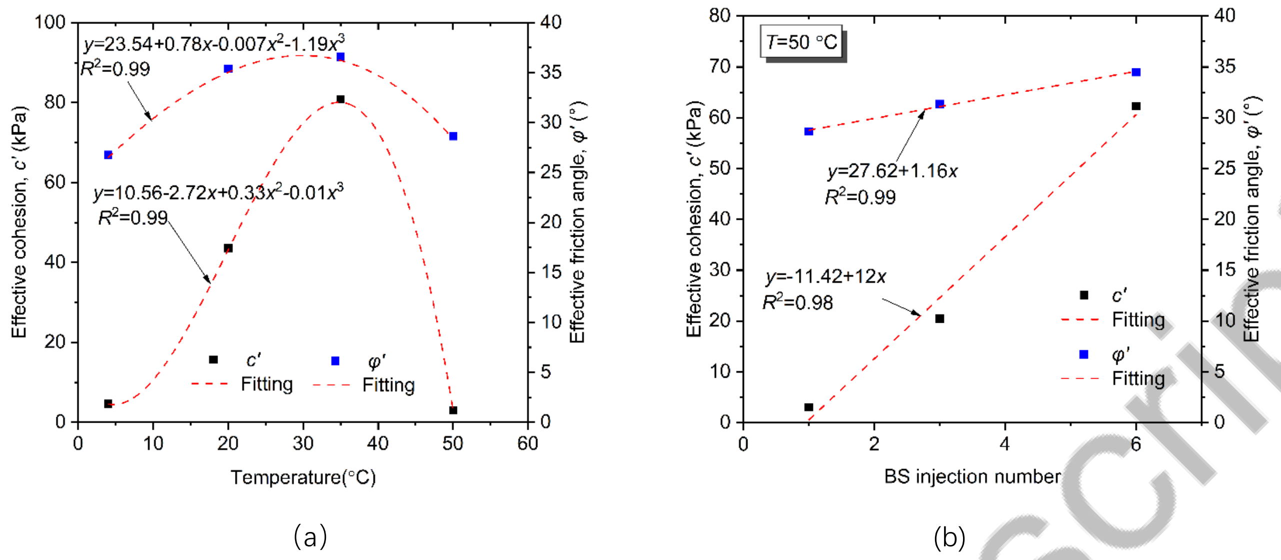

Figure 8 Relationship between strength parameters and average CaCO3 content at (a) different temperature; (b) different BS injection numbers at 50℃(1)

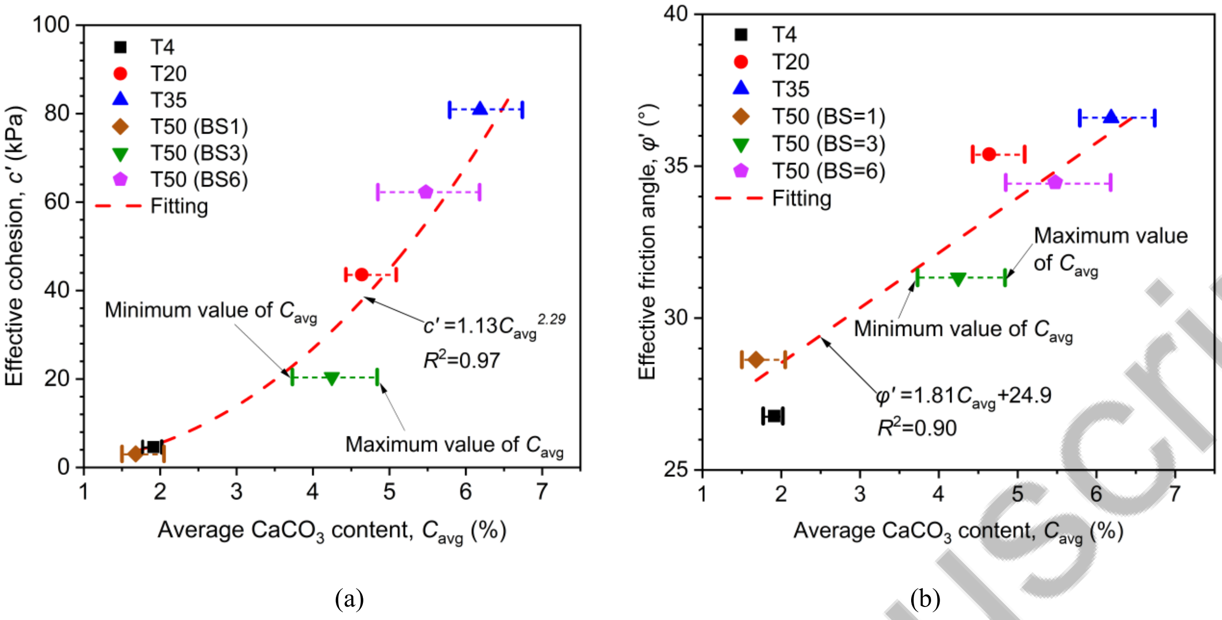

Figure 9 Effects of average $CaCO_3$ content on (a) effective cohesion; and (b) friction angle.

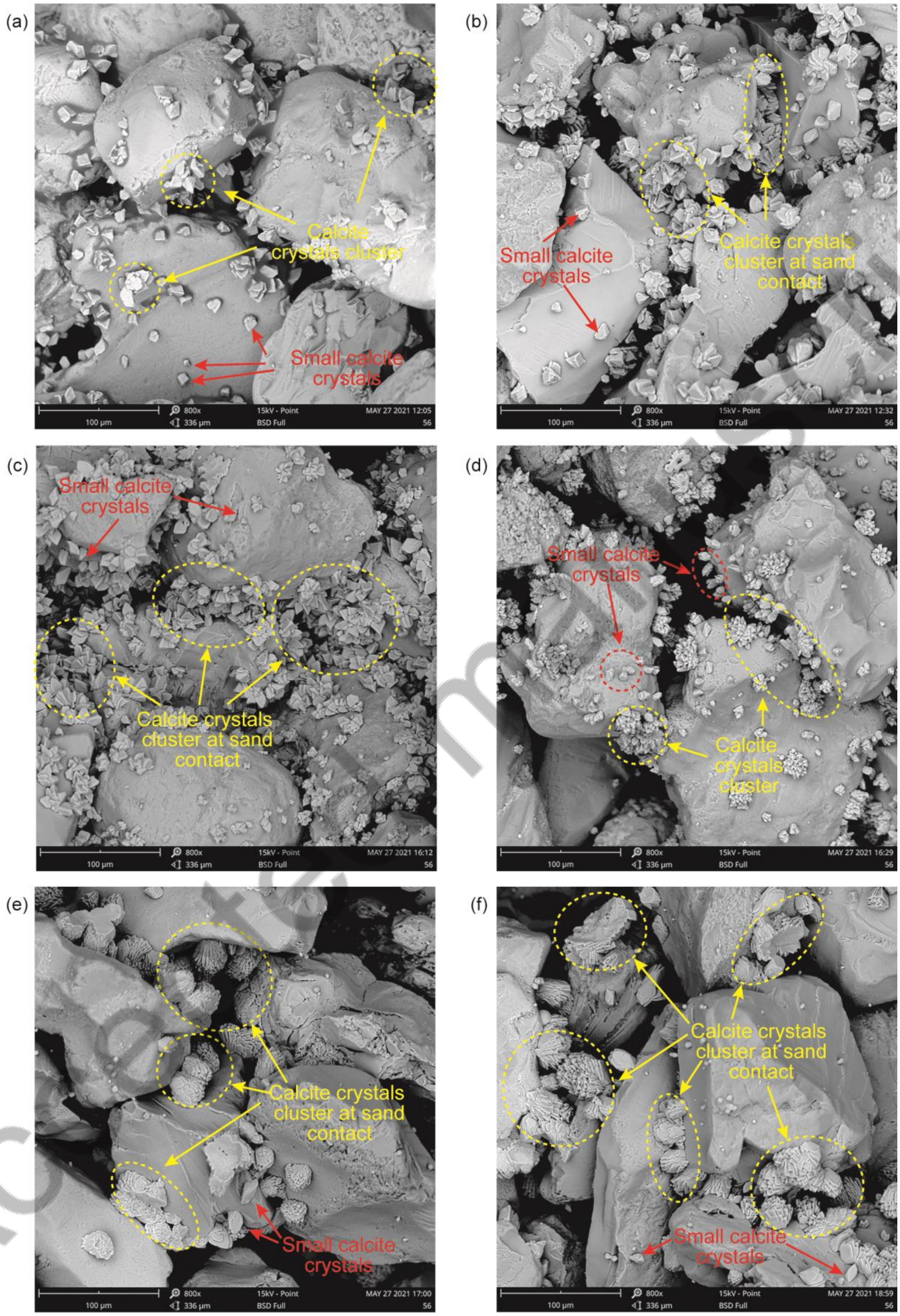

Figure 10 SEM images of specimens treated at different temperatures: (a) T=4℃ (BS1); (b) T=20℃ (BS1); (c) T=35℃ (BS1); (d) T=50℃ (BS1); (e) T=50℃ (BS3); (f) T=50℃ (BS6)

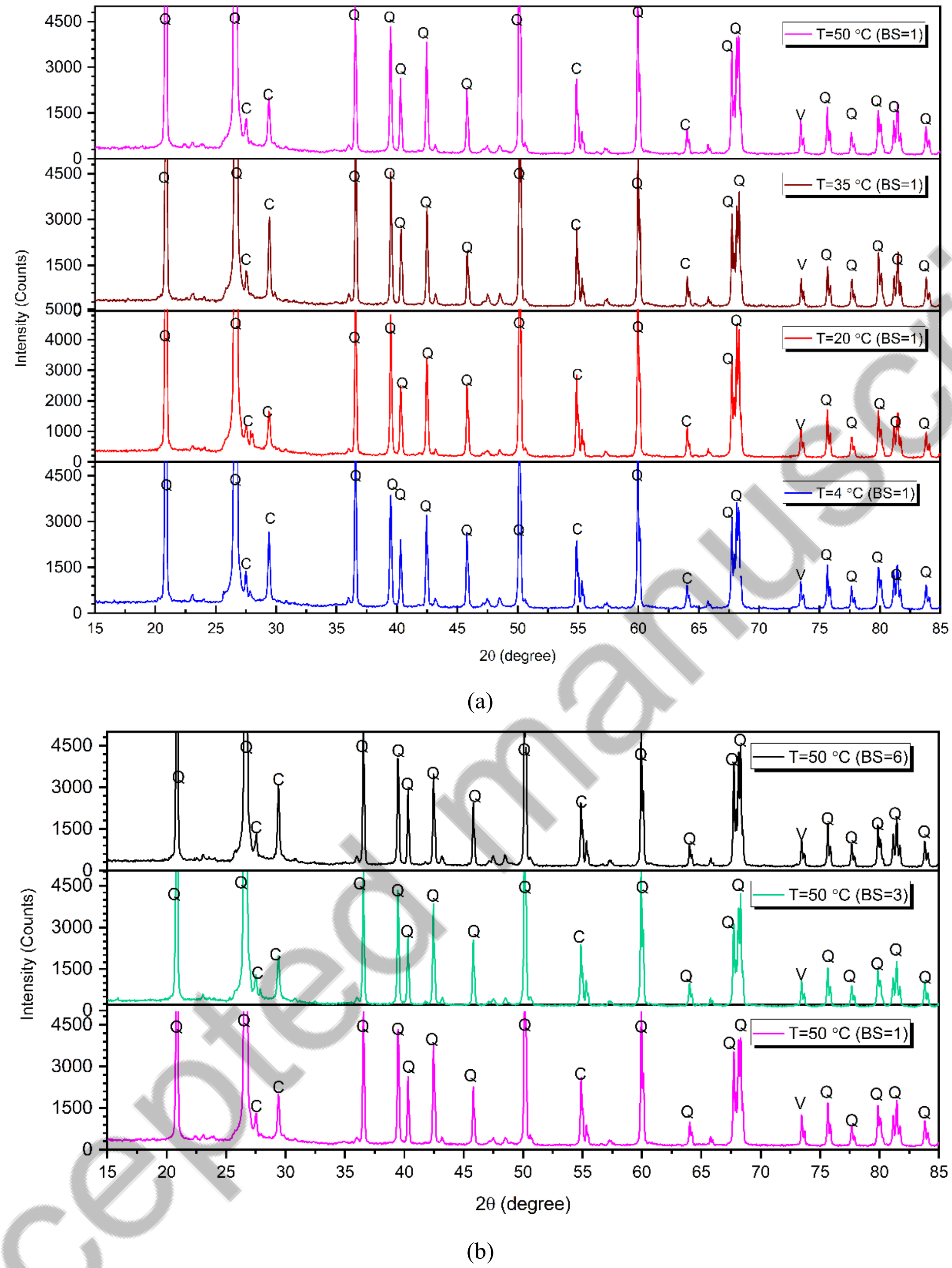

Figure 12 The XRD results of biocemented sand at: (a) different temperatures; and (b) different BS injection number at 50°C; Q indicates Quartz, Ca indicates calcite.

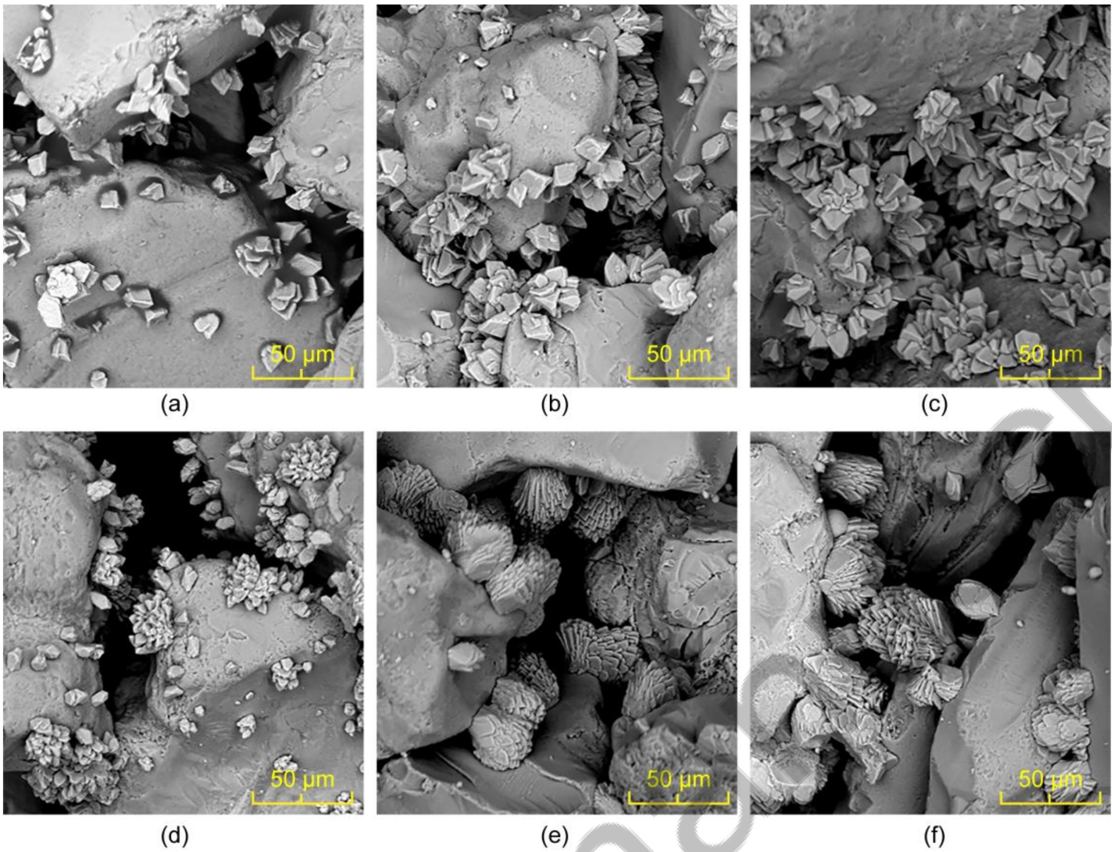
50 µm
50 µm
50 µm
(a)
(b)
(c)
50 µm
50 µm
50 µm
(d)
(e)
(f)

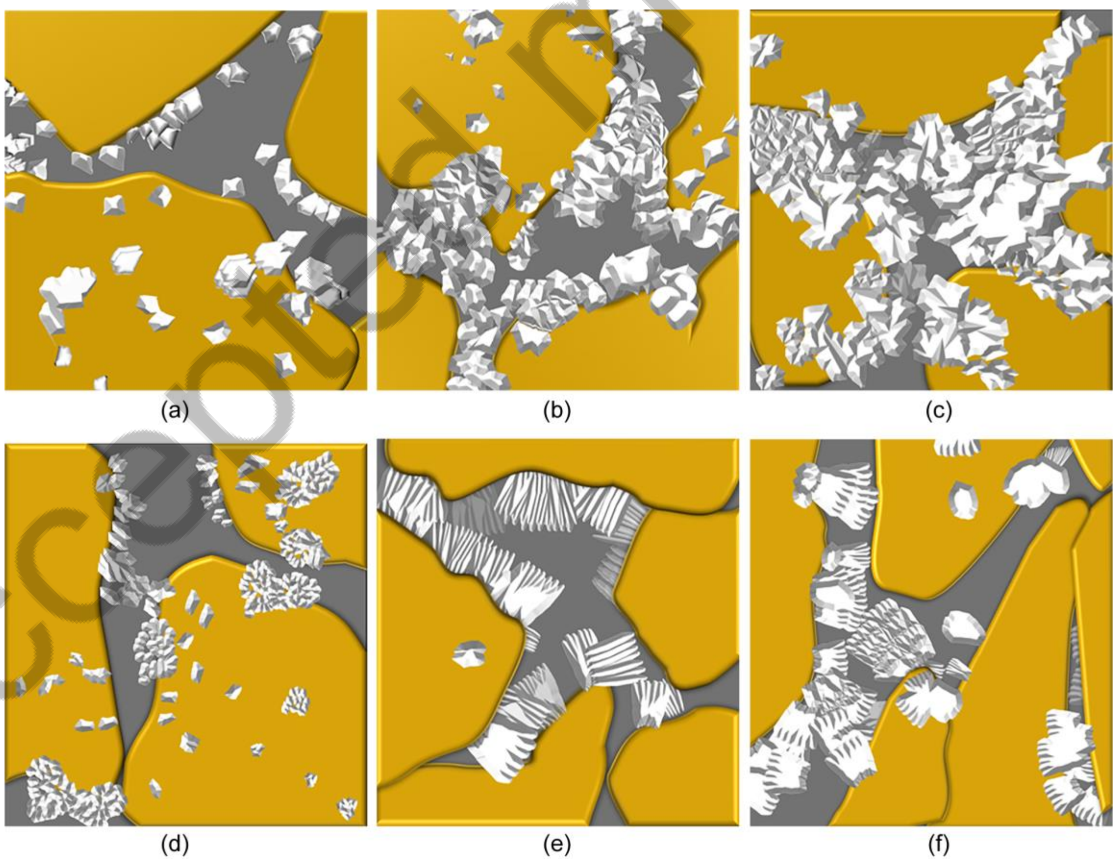
(a)
(b)
(c)
(d)
(e)
(f)

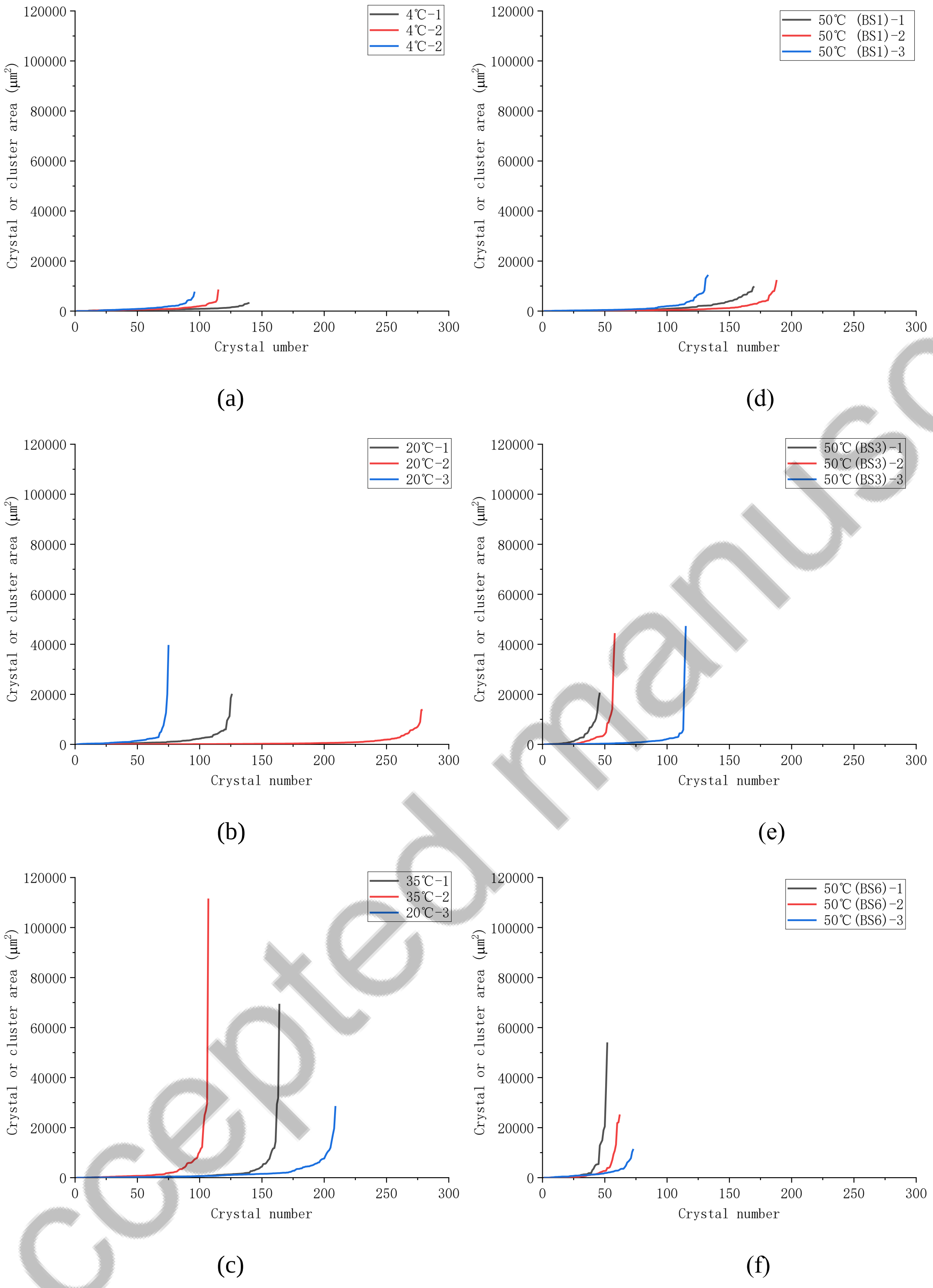
4℃-1
4℃-2
4℃-2
Crystal or cluster area (μm²)
Crystal umber
(a)
50℃ (BS1)-1
50℃ (BS1)-2
50℃ (BS1)-3
Crystal or cluster area (μm²)
Crystal number
(d)
20℃-1
20℃-2
20℃-3
Crystal or cluster area (μm²)
Crystal number
(b)
50℃ (BS3)-1
50℃ (BS3)-2
50℃ (BS3)-3
Crystal or cluster area (μm²)
Crystal number
(e)
35℃-1
35℃-2
20℃-3
Crystal or cluster area (μm²)
Crystal number
(c)
50℃ (BS6)-1
50℃ (BS6)-2
50℃ (BS6)-3
Crystal or cluster area (μm²)
Crystal number
(f)

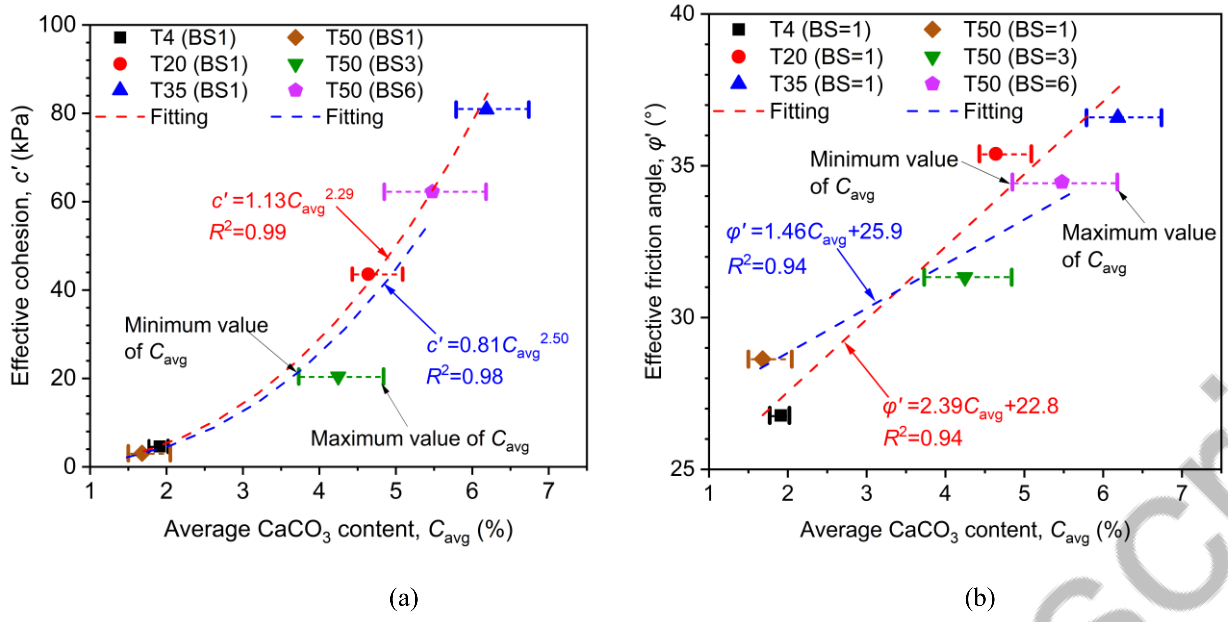

Figure 14 Effects of average $CaCO_3$ content on (a) effective cohesion; and (b) friction angle.

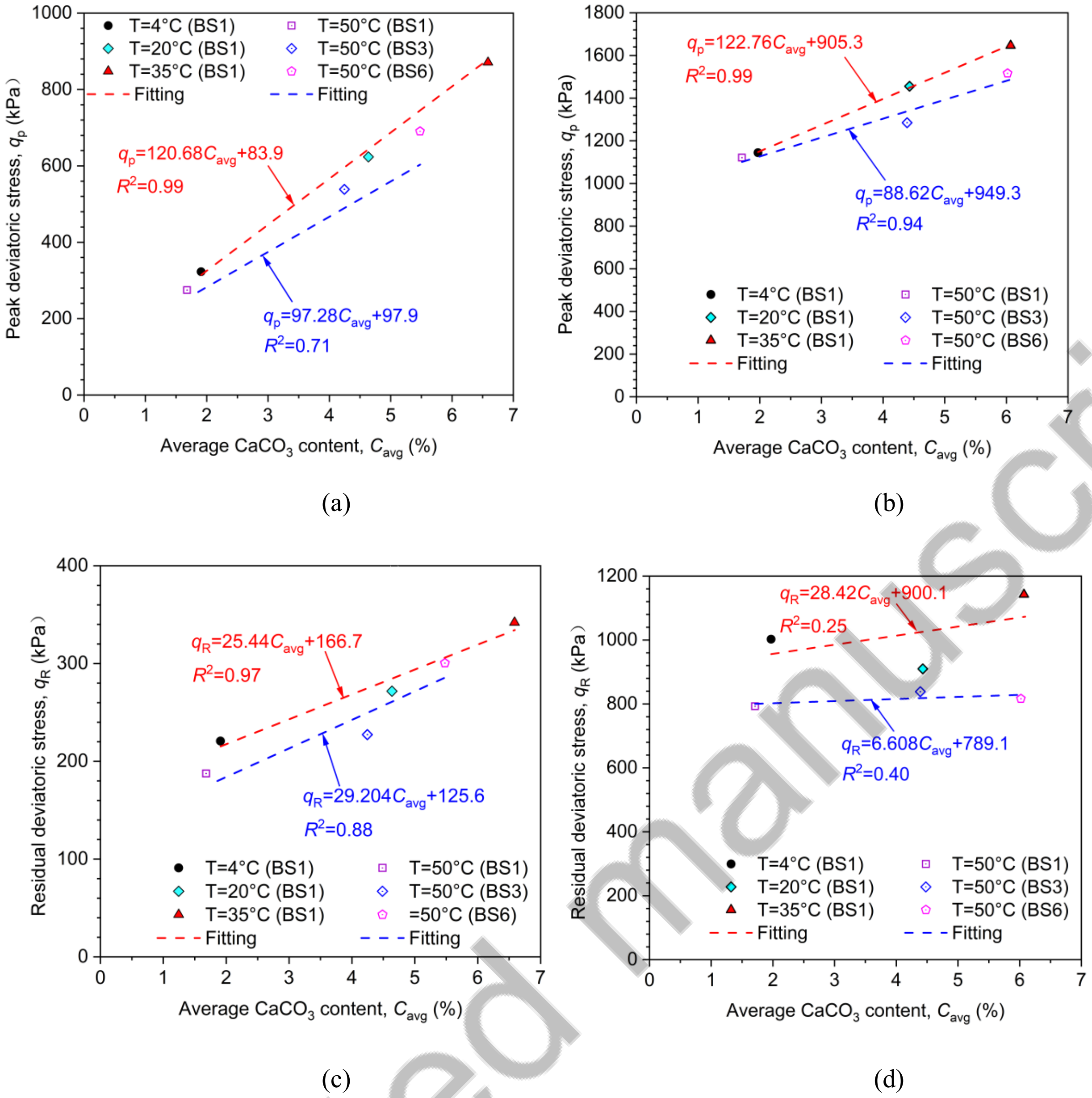

Figure 15 Effects of average $CaCO_3$ content on peak strength (a, c) and residual strength (b, d) at 100 kPa (a, c); and 400 kPa (b, d)